Non-invasive diagnosis and follow-up of right ventricular overload

Henkens, I.R.

VI

Improved ECG detection of presence and severity of right ventricular pressure load validated with cardiac magnetic resonance imaging

Ivo R. Henkens

Koen T.B. Mouchaers

Anton Vonk Noordegraaf

Anco Boonstra

Cees A. Swenne

A.C. Maan

Sum-Che Man

Jos W.R. Twisk

Ernst E. van der Wall

Martin J. Schalij

Hubert W. Vliegen

Am J Physiol Heart Circ Physiol 2008;294:H2150-7

Abstract

Background

The study aimed to assess whether the 12-lead electrocardiogram (ECG) derived ventricular gradient, a vectorial representation of ventricular action potential duration heterogeneity directed towards the area of shortest action potential duration, can improve ECG diagnosis of chronic right ventricular (RV) pressure load.

Methods

We compared ECGs from 72 pulmonary arterial hypertension patients recorded <30 days before onset of therapy with ECGs from matched healthy controls subjects (n=144). We compared conventional ECG criteria for increased RV pressure load with the ventricular gradient.

Results

In 38 patients a cardiac magnetic resonance (CMR) study had been performed within 24 hours of the ECG. By multivariable analysis, combined use of conventional ECG parameters (rsr'or rsR' in V1, R/S>1 with R>0.5 mV in V1, and QRS axis >90º) had a sensitivity of 89%, and a specificity of 93% for presence of chronic RV pressure load. However, the ventricular gradient not only had a higher diagnostic accuracy for chronic RV pressure load by ROC analysis (AUC=0.993, SE 0.004 vs. AUC=0.945, SE 0.021, $P<0.05$), but also discriminated between mild to moderate and severe RV pressure load. CMR identified an inverse relation between the ventricular gradient and RV mass, and a trend to a similar relation with RV volume.

Conclusions

Chronically increased RV pressure load is electrocardiographically reflected by an altered ventricular gradient associated with RV remodeling related changes in ventricular action potential duration heterogeneity. Using the ventricular gradient allows ECG detection of even mildly increased RV pressure load.

Introduction

Moderately increased chronic right ventricular (RV) pressure load is hard to detect non-invasively due to the position and mass of the RV [1-3]. Conventional 12-lead electrocardiographic (ECG) parameters of increased RV pressure load lack diagnostic accuracy, precluding their use for screening purposes [4-8]. Partly because the chest electrodes predominantly overly the left ventricle, partly because the 12-lead ECG renders 12 separate one-dimensional projections of the three-dimensional (3D) cardiac vector in time [9], but not in the least because the RV mass is relatively low compared to the left ventricular (LV) mass. This scalar ECG representation hampers the direct appreciation of the ECG as a recording of a 3D process. However, a synthesized vectorcardiogram can be easily derived mathematically from the ECG allowing the calculation of electrocardiographic 3D parameters. One of these parameters is the ventricular gradient (VG), a 3D measure of ventricular action potential duration (APD) heterogeneity oriented from the area with the longest APD towards the area with the shortest APD [10, 11]. The VG (mV·ms) is the sum of the 3D integrals of both the QRS complex and the T-wave (net area subtended by the heart vector over the QRS complex and the T-wave) [10, 11]. A change in magnitude and/or orientation of the VG signifies a change in APD heterogeneity [10, 12]. APD changes due to chronic RV pressure load must therefore change the VG [12]. In a rat model we recently demonstrated that the VG changes markedly during the development of pulmonary arterial hypertension (PAH), a model of chronic RV pressure load [13]. We therefore decided to study the use of the VG in diagnosing chronic RV pressure load. In humans however, comparison of ECGs at the time of diagnosis of PAH with ECGs from a disease-free state is in general not feasible, since PAH remains undetected for a long time [14]. ECGs from PAH patients were therefore compared with ECGs from healthy controls. To further appreciate the diagnostic potential of the VG in chronic RV pressure load, all ECGs were also evaluated for the conventional criteria of increased right heart load [15].

Methods

Patients

The study complies with the Declaration of Helsinki. Patient data were gathered as part of routine clinical care in the VU University Medical Center and analyzed retrospectively. Healthy control subjects gave written informed consent for this study that was approved by the institutional ethical review board of the Leiden University Medical Center.

Between December 1999 and December 2005, 565 consecutive patients were evaluated

with a right heart catheterization because of suspected PAH, defined as a mean pulmonary artery pressure >25 mmHg and pulmonary capillary wedge pressure <15 mmHg. PAH was considered to be idiopathic when identifiable causes for pulmonary hypertension (i.e. congenital heart disease, portal hypertension, collagen vascular disease, HIV infection, left heart disease, hypoxic pulmonary disease or chronic thrombo-embolic disease) were excluded [8, 16]. One hundred and ten patients were identified with idiopathic PAH. A digitally stored ECG recorded within 30 days prior to diagnostic right heart catheterization was available in 72 patients (15 male).

Right heart catheterization

All PAH patients underwent right heart catheterization, during which right atrial pressure, pulmonary artery pressure, pulmonary capillary wedge pressure, and mixed venous oxygen saturation were measured. Cardiac output was calculated using Fick's principle. Oxygen consumption was measured during right heart catheterization. Pulmonary vascular resistance ($mmHg \cdot L^{-1} \cdot min^{-1}$) was calculated by dividing the transpulmonary gradient (pressure difference between mean pulmonary artery pressure and pulmonary capillary wedge pressure) by cardiac output.

ECG analysis

Conventional 10-second ECGs were recorded by certified ECG technicians with patients in supine position using the standard 12-lead electrode configuration. ECGs were recorded on commercially available electrocardiographs (MAC VU and MAC 5000, GE Healthcare, The Netherlands, and Megacart, Siemens, Germany, respectively), at a paper speed of 25 $mm \cdot s^{-1}$; sensitivity 1mV=10mm; sample frequency of 500 Hz. All ECGs were assessed for the presence of conventional 12-lead ECG criteria of RV hypertrophy [15]. ECGs were also analyzed with LEADS, our non-commercial, research oriented ECG analysis program which automatically renders amplitudes, areas and vector directions [17]. In short, LEADS automatically selects beats for averaging based on signal quality criteria (baseline, noise). This selection of beats is then reviewed and edited by the investigator. The thus selected beats are then averaged by LEADS. After manually reviewing and editing the onset and end of the QRS-complex, a synthesized vectorcardiogram is generated with the inverse Dower matrix [17, 18]. Parameters derived from this vectorcardiogram, such as the VG magnitude ($mV \cdot ms$) and spatial orientation (azimuth°, orientation in the transversal plane, and elevation°, deviation from the transversal plane), are then calculated. The VG is defined as: $\int H(t) \cdot dt$ in which H(t) is the heart vector, as represented in the X,Y, and Z leads of the vectorcardiogram [19]. This integral, taken over the

QRST interval, is non-zero due to action potential morphologic differences in the ventricles, most often thought of as APD differences [10]. Orientation of the axes is in accordance with the American Heart Association recommendations: X axis positive from right to left, Y axis positive in cranio-caudal direction, and Z axis positive in antero-posterior direction [20]. Control ECGs were selected from a large database of healthy students of the Leiden University Medical Faculty. All ECGs were scrutinized for normality according to the Minnesota criteria by an experienced cardiologist [21]. Prior to the use of the selected ECGs for comparison in this study, all ECGs were anonymized. All ECGs were analyzed twice by the first author (IRH), and a third time by the second author (KTBM) to determine the intra-observer and inter-observer variability for calculating the VG. As the VG depends on heart rate [22] and gender, but not on age (unpublished data), we matched each patient ECG for heart rate and gender with two ECGs from healthy subjects.

Cardiac magnetic resonance imaging

In 38 patients CMR imaging had been performed on a Siemens 1.5 T Sonata scanner (Siemens Medical Solutions, Erlangen, Germany) within 24 hours of the ECG recording, as previously described [23]. Cardiac short-axis cine images of both RV and left ventricle (LV) were acquired from base to apex at 10 mm slice distance. A blinded observer delineated RV and LV endocardial and epicardial contours manually, and MASS software (Dept. of Radiology, Leiden University Medical Center, Leiden, the Netherlands) was used to obtain RV and LV mass ratios and RV and LV end-diastolic volume ratios.

Statistical analysis

The SPSS for Windows Software package (version 12.0.1, SPSS Inc, Chicago Illinois) was used for data analysis. Normally distributed values are presented as means ± standard deviations. Independent t-tests were used for comparison of PAH patients and healthy controls. Comparison of three categories was performed with one-way analysis of variance with post-hoc Bonferroni correction. To determine the discriminative power of dichotomous variables for diagnosing PAH, cross tabulations were used for determination of sensitivity and specificity. To determine the diagnostic value of vectorcardiogram-derived parameters compared to conventional electrocardiographic parameters we used a receiver operating characteristic (ROC) analysis. Areas under the curve (AUC) were compared using the method proposed by Hanley and McNeil [24], which corrects for existing correlations between ROC curves derived from the same cases. Binary logistic regression analysis was used to determine the optimal model for classification of increased RV afterload for both ECG-derived variables and vectorcardiogram-

derived variables. Subsequently the optimal model was used in a bootstrapping analysis to determine the accuracy of the odds ratio (OR) in this classification model. Pearson correlation analysis was used for analysis of intra-observer and inter-observer variability, as well as for comparison of the VG with CMR derived variables of RV mass, and volume. A value of $P<0.05$ was considered to be statistically significant.

Results

Patient characteristics at the time of the diagnostic right heart catheterization are presented in Table 1. Controls (n=144, 30 male) were younger than patients (mean age: 19.7 ± 1.3 years vs. 43.7 ± 22.8 years, $P<0.001$). Mean heart rate was 82·min^{-1} ± 17·min^{-1} in PAH patients vs. 80·min^{-1} ± 14·min^{-1} in controls ($P=0.47$). Calculation of the VG proved to be highly reproducible, with both excellent intra-observer (r=0.994, $P<0.001$) and inter-observer agreement (r=0.992, $P<0.001$).

Typical examples of RV and pulmonary artery pressures (PAP) with the corresponding ECG and vectorcardiogram findings are presented in Figure 1 for a healthy subject (catheterized for exclusion of familial PAH after inconclusive transthoracic contrast echocardiography), a patient with moderate PAH, and a patient with severe PAH. It can be appreciated from leads I and aVF that an intermediate frontal plane QRS axis is present in the subject without PAH as well as in the patient with moderate PAH, whereas a right axis deviation is present in the patient with severe PAH. Furthermore, lead V1 is within normal limits for both the subject without PAH and the patient with moderate PAH, whereas lead V1 qualifies for RV hypertrophy in the patient with severe PAH: R>S and R>5 mm, initial P wave>1mm high and wide, and the T wave is discordant with the QRS, reflecting RV strain. A closer look at the projection of the VG on the X, Y, and Z axes reveals that the VG projection on the X axis (net QRST area in the X lead) becomes smaller proportional to the degree of chronic RV pressure load. The lower

Table 1: PAH patient characteristics (n=72, 15 male)

Characteristic	Mean
RAP (mmHg)	9 ± 6
Mean PAP (mmHg)	56 ± 14
PCWP (mmHg)	7 ± 4
PVR (mmHg·L^{-1}·min^{-1})	13.4 ± 7.2
Mixed venous SpO_2 (%)	63 ± 10
Cardiac index (L·m^{-2}·min^{-1})	2.3 ± 0.9

RAP = right atrial pressure, Mean PAP = mean pulmonary artery pressure, PCWP = pulmonary capillary wedge pressure, PVR = pulmonary vascular resistance, SpO_2 = oxygen saturation in blood.

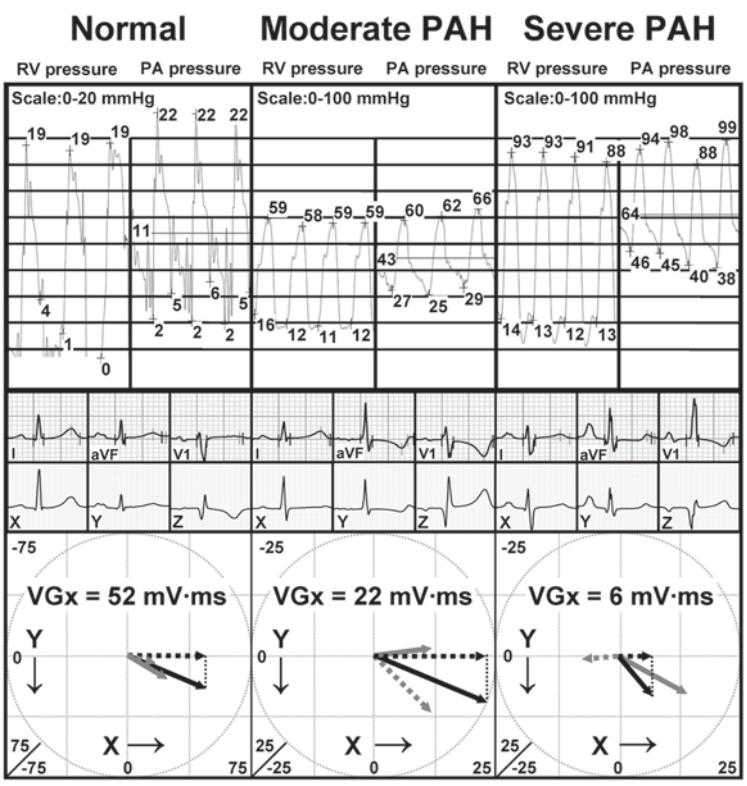

Figure 1

The effect of different levels of chronic RV pressure load on the ECG and vectorcardiogram is illustrated in a patient without PAH (catheterized for exclusion of familial PAH after inconclusive transthoracic contrast echocardiography; left), a patient with moderate PAH (middle), and a patient with severe PAH (right), respectively. Top panels: RV and pulmonary artery pressures (PAP). Horizontal lines: mean PAP; mean PAP=11 mmHg in the patient without PAH, mean PAP=43 mmHg in the patient with moderate PAH, and mean PAP=64 mmHg in the patient with severe PAH. Of note: the pressure scale is set at 0 - 20 mmHg in the control subject with normal RV pressure load, whereas the pressure scale is set at 0 - 100 mmHg in the patients with moderate and severe PAH. Second row panels: corresponding ECG leads I, aVF, and V1; no ECG abnormalities are present in the patient with moderate PAH, despite a chronically elevated RV pressure load. Third row panels: the VG projections (QRST integral) on the X, Y, and Z axis, revealing that the VG projection on the X axis gradually becomes smaller, proportionate to the degree of chronic RV pressure load. The relation between the QRS integral, the T wave integral and the VG is illustrated in the bottom row for the VG projection on the X axis (VGx) in the frontal plane. The VG (solid black line) is the vectorial sum of the QRS (dashed grey line) and T (solid grey line) integrals. VGx is the projection of the VG on the X axis (dashed black line). Of note: all numbers in the bottom panels are expressed in mV·ms, with a scale of 0 - 75 mV·ms for the control subject with normal RV pressure load, and a scale of 0 - 25 mV·ms for the patients with moderate and severe PAH.

Table 2: Difference in ECG derived variables between controls and patients with moderate or severe PAH

	Controls (n=144)	Mild to Moderate PAH (n=16)	Severe PAH (n=56)	Controls vs. Mild to Moderate PAH	Controls vs. Severe PAH	Mild to Moderate PAH vs. Severe PAH
ECG variables	Mean ± SD	Mean ± SD	Mean ± SD	*P*	*P*	*P*
QRS	38.5 ± 13.8	24.3 ± 10.9	28.6 ± 16.2	0.001	<0.001	NS
T	68.4 ± 25.2	31.2 ± 13.3	37.4 ± 19.3	<0.001	<0.001	NS
VG	85.9 ± 27.6	34.1 ± 17.1	35.0 ± 17.8	0.001	<0.001	NS
QRS-X	22.4 ± 10.1	4.4 ± 9.6	-2.9 ± 11.1	<0.001	<0.001	0.040
QRS-Y	21.2 ± 10.5	15.3 ± 9.3	14.4 ± 13.3	NS	<0.001	NS
QRS-Z	18.8 ± 12.5	12.1 ± 12.0	-2.7 ± 23.9	NS	<0.001	0.005
T-X	46.6 ± 19.2	15.0 ± 12.9	6.9 ± 18.5	<0.001	<0.001	NS
T-Y	21.6 ± 12.6	5.9 ± 16.5	-0.5 ± 22.3	0.001	<0.001	NS
T-Z	-40.9 ± 21.8	1.6 ± 22.2	18.9 ± 23.4	<0.001	<0.001	0.020
VG-X	68.1 ± 22.0	17.5 ± 15.0	2.8 ± 16.1	<0.001	<0.001	0.033
VG-Y	42.7 ± 17.8	21.2 ± 12.5	14.7 ± 20.6	<0.001	<0.001	NS
VG-Z	-20.4 ± 21.9	12.9 ± 13.0	13.8 ± 21.4	<0.001	<0.001	NS
QRS-T(º)	71.5 ± 23.5	97.5 ± 45.9	105.2 ± 38.6	0.004	<0.001	NS

QRS, T, and QRST integrals (the latter denoted as ventricular gradient, VG). "-X", "-Y", "-Z": projections on the X, Y, and Z axis, respectively (all in mV·ms). QRS-T(º): spatial angle between the QRS and T integrals.

panels illustrate also that chronic RV pressure load leads to a proportionate decrease in QRS and T integral vectors, and to an increase in QRS-T spatial angle (Table 2), together resulting in a smaller and differently oriented VG.

In general, conventional ECG criteria had low diagnostic accuracy for presence of increased RV afterload (Table 3). With a sensitivity of 84% and a specificity of 96%, a QRS axis >90º in the frontal plane was the conventional ECG parameter with the highest individual diagnostic accuracy for chronically increased RV pressure load (Table 3). Multivariable binary logistic regression analysis performed in a backward stepwise fashion (removal if $P>0.10$, inclusion if $P<0.05$, a priori chance of PAH=0.33) rendered the following formula for optimal prediction of presence of PAH: y = 2.204 · (presence of rSr' or rSR' in lead V1) + 3.079 · (presence of R:S>1 in lead V1 with R>0.5mV) + 4.542 · (presence of QRS axis >90º) - 6.679 (sensitivity=89%, specificity=94%, $P<0.001$). Although sensitivity and specificity did not differ importantly between the prediction based on a multivariable analysis compared to the single prediction of the presence of QRS axis>90º, the multivariable prediction showed

Table 3: Diagnosis of chronically increased RV pressure load with conventional ECG criteria

ECG criterion	Sensitivity (%)	Specificity (%)	Correct diagnosis in all 216 subjects (%)
P>0.25 mV in lead II	30	91	71
qR pattern in lead V1	36	100	79
rSR' pattern in lead V1	18	96	70
R in lead aVR>0.5 mV	14	100	71
R:S>1 in lead V1 with R>0.5 mV	51	98	82
R in lead V1 + S in lead V5>1 mV	53	94	80
R:S<1 in lead V5 or V6	24	99	74
R≤0.4 mV in lead V5 or V6 with S=<0.2mV in lead V1	13	100	71
S in lead I and Q in lead III	49	70	63
S wave in leads I, II, and III	28	74	59
S in lead V5 or V6=>0.7 mV	31	98	76
Inverted T wave in lead V1	69	62	64
QRS axis >90°	84	96	92

The "P" denotes the deflection caused by atrial depolarization. The "Q" denotes an initial negative deflection, the "R" is the first positive wave, and the first negative wave after a positive wave is the S wave. A second upright wave following an S wave is an R' wave. Tall waves (>0.5 mV) are denoted by capital letters and smaller ones by lowercase letters. Together, the QRS complex reflects ventricular depolarization. The T wave denotes the deflection caused by ventricular repolarization.

a larger AUC than QRS axis>90º alone (Figure 2).

Significant differences in the VG were observed, however, between PAH patients and healthy controls. In general, in PAH patients the VG assumed a different orientation from healthy controls and was also considerably smaller: 34.8 ± 17.5 mV·ms vs. 85.9 ± 27.6 mV·ms (P<0.001) (Figure 3). It is easily appreciated from the right lower panel that VG magnitude alone can not accurately separate PAH patients and healthy controls. Multivariable analysis showed that a combination of VG magnitude and orientation had superior discriminating power to either variable alone, especially the VG projection on the X axis. Multivariable analysis in a stepwise forward fashion (inclusion if P<0.01, removal if P>0.05) including the respective orthogonal projections of the mean QRS integrals, mean T-wave integrals, and the mean VGs, illustrated that of all the significantly related single variables the VG projection on the X axis was the variable with the highest discriminating power (Table 2). PAH patients and controls were therefore compared for the VG projection on the X axis. Receiver-operating-curve analyses for diagnosis of increased RV pressure load are presented in Figure 3. The VG magnitude

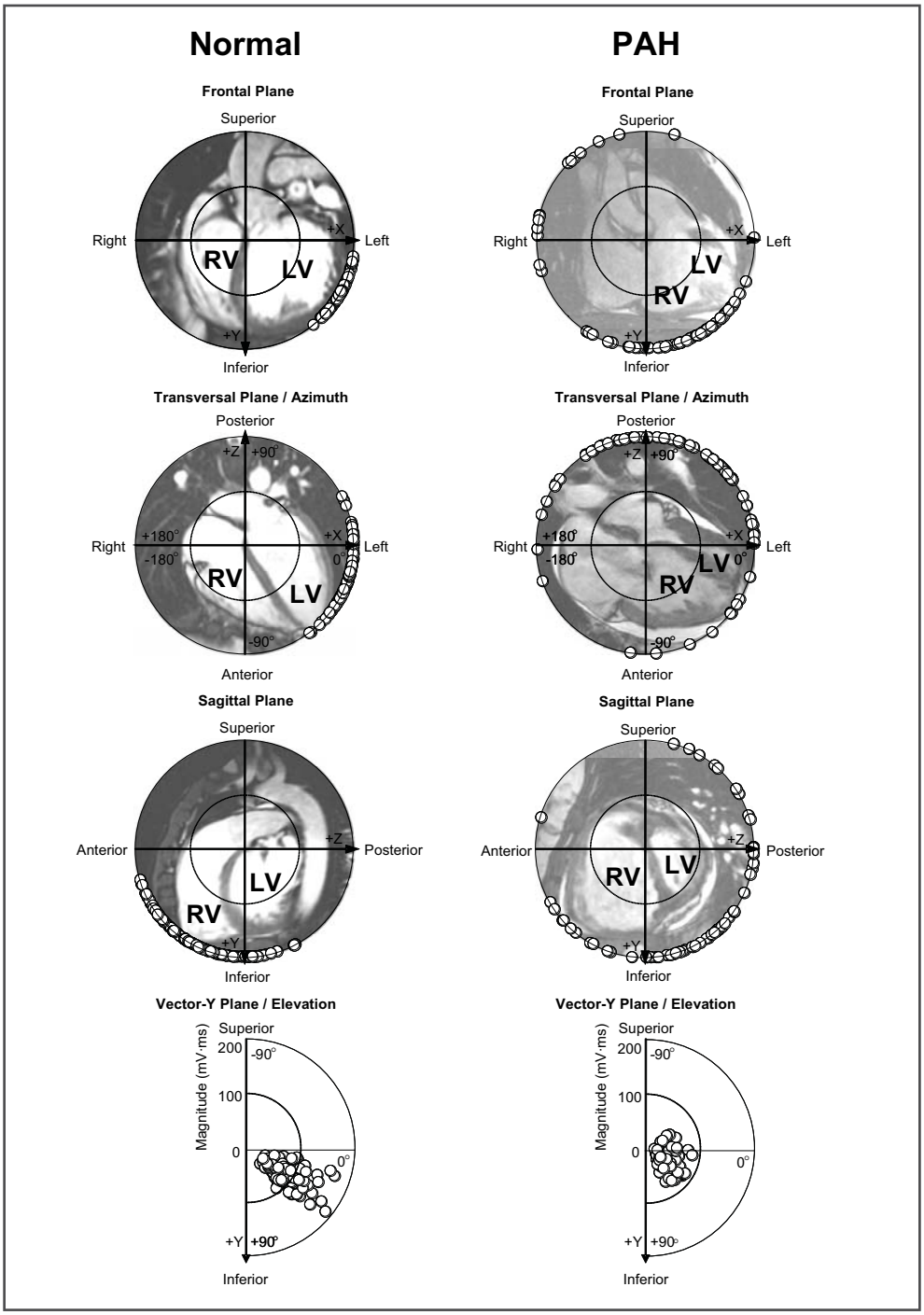
Normal
PAH
Frontal Plane
Superior
Right
Left
Inferior
RV
LV
+X
+Y
Transversal Plane / Azimuth
Posterior
Anterior
+Z
+90°
+180°
-180°
0°
-90°
Sagittal Plane
Vector-Y Plane / Elevation
Magnitude (mV·ms)
200
100
0

◄ Figure 2

Superimposed representations of the spatial orientation of all individual VG vectors in the frontal, transversal and sagittal planes, and of the VG vector magnitude in the Vector-Y plane. Left-side plots: normal subjects; right-side plots: PAH patients. Insets are frontal, transversal and sagittal MRI slices of one arbitrarily chosen normal subject (left) and PAH patient (right). The MRI insets are chosen in such a way that the AV-node area is in the origin, which parallels the usual vectorial representation of the electrical heart activity. VG azimuths can be directly appreciated in the transversal plane, while the VG magnitudes and elevations can be directly appreciated in the Vector-Y plane. Of note, this Vector-Y plane is a different plane for each vector; therefore, there is no representative MRI slice that can serve as an inset for the Vector-Y plane. All VG-Y planes have been superimposed to allow comparison of all VG magnitudes and elevations. These images illustrate that although in normals there is considerable heterogeneity in both VG orientation and magnitude, the VG orientation is quite different in PAH patients and VG magnitude is generally lower. Due to the heterogeneity of disease severity among PAH patients the VG orientation and VG magnitude varies considerably among PAH patients.
'O'=an individual VG

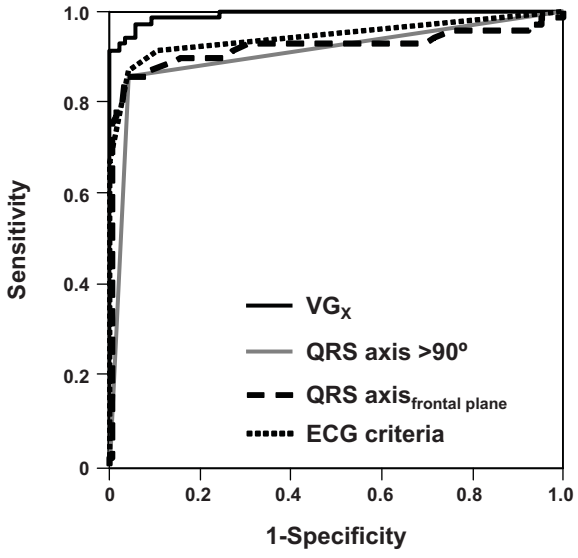

Figure 3

Receiver operating characteristics (ROC) curves for diagnosis of increased RV pressure load. Solid black line: ROC of the VG projection on the X axis (continuous variable; AUC=0.993). Solid grey line: ROC of the presence of a QRS axis >90º in the frontal plane (dichotomous variable; AUC=0.900). Coarse dashed line: ROC of the QRS axis in the frontal plane (continuous variable; AUC=0.904). Fine dashed line: ROC of the composite model of conventional ECG criteria: y=2.204·(presence of rSr' or rSR' in lead V1) + 3.079·(presence of R:S>1 in lead V1 with R>0.5mV) + 4.542·(presence of QRS axis >90º) - 6.679 (AUC=0.945).

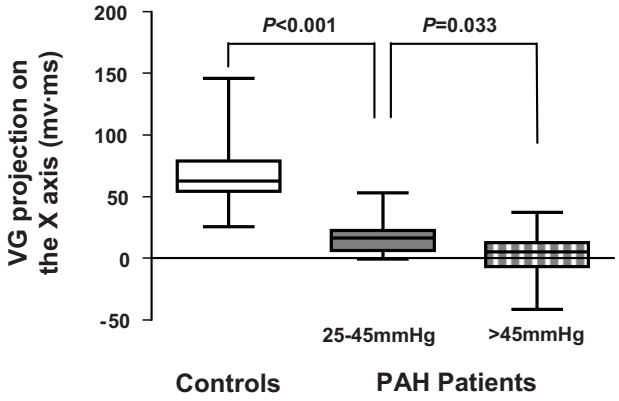

Figure 4

In healthy controls (assumed mean PAP<25 mmHg, n=144) the VG projection on the X axis is much larger than in patients with a chronically increased RV pressure load (mean PAP>25 mmHg, n=72). Furthermore, the VG projection on the X axis allows distinction between a mildly to moderately elevated RV pressure load (mean PAP=25-45 mmHg) and a severely elevated RV pressure load (mean PAP>45 mmHg, n=56).

projection on the X axis (AUC=0.993) had a significantly larger AUC than presence of a QRS axis >90º (dichotomous variable; AUC=0.900, z-score=3.36, $P<0.01$), QRS axis in the frontal plane (continuous variable; AUC=0.904, z-score=2.89, $P<0.01$), and the composite model of conventional ECG parameters (AUC=0.945, z-score=2.27, $P<0.05$). Binary logistic regression analysis rendered the following formula for prediction of presence of increased RV pressure load by the X component of the VG: $y = -0.195 \cdot VGx + 6.195$ (OR=0.82 for each unit increase in VG projection on the X axis) with a sensitivity of 97% and a specificity of 94%. Bootstrapping analysis validated the adequacy of this model, rendering a 95% confidence interval for the OR of 0.74-0.91 ($P<0.001$) based on a normal distribution of the regression coefficients over the bootstrap samples. To assess whether the VG projection on the X axis could differentiate between mild to moderate and severe PAH, patients were stratified in two categories according to mean pulmonary artery pressure (mean PAP) level: mean PAP=25-45 mmHg (n=16), and mean PAP>45 mmHg (n=56). Figure 4 illustrates that the VG projection on the X axis was already markedly decreased in patients with mildly to moderately increased RV pressure load (mean PAP=25-45 mmHg), and even more in patients with a severely increased RV pressure load (mean PAP>45 mmHg). One-way analysis of variance showed that PAH patients with a mean PAP=25-45 mmHg had a VG projection on the X axis that was significantly lower than in controls (17.5 ± 15.0 mV·ms vs. 68.1 ± 22.0

mV·ms, $P<0.001$), but still higher than in PAH patients with a mean PAP>45 mmHg (17.5 ± 15.0 mV·ms vs. 2.8 ± 16.1 mV·ms, $P=0.033$). Here too, the projection of the VG on the X axis was best discriminating, since the VG magnitude alone did not differentiate between patients with a mean PAP=25-45 mmHg and patients with a mean PAP>45 mmHg, although VG magnitude in both groups of PAH patients was lower than in controls (Table 2.) Since the VG is the vectorial sum of the QRS and T integrals, projections of QRS and T integrals as well as the QRS-T spatial angle were also calculated. Mean QRS integral and mean T-wave integral magnitudes and projections on the X, Y, and Z axes were generally different between controls and PAH patients, although the distinction between mild to moderate PAH and severe PAH could only be made by QRS integral projections on the X and Z axis, the T-wave integral projection on the Z axis, and again the VG projection on the X axis (Table 2). Overall the QRS-T spatial angle was higher in patients with a chronically increased RV afterload than in controls, signifying that there is a higher degree of discordance between depolarization and repolarization in PAH patients (Table 2).

CMR showed that RV mass was related to the VG projection on the X axis (Figure 5A), and a trend was observed towards a relation between a higher RV volume and a smaller VG projection on the X axis (Figure 5B).

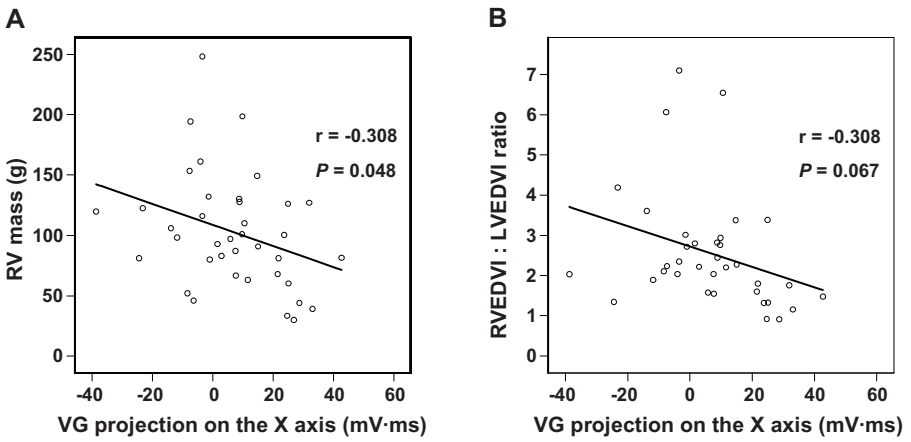

Figure 5

A. RV mass showed an inverse relation with the VG projection on the X axis (r=-0.323, P=0.048)

B. There was a trend toward a similar inverse relation between a higher RV end-diastolic volume and the VG projection on the X axis (r=-0.308, P=0.067). RVEDVI=RV end-diastolic volume indexed for body surface area. LVEDVI=LV end-diastolic volume indexed for body surface area.

Discussion

The key finding of this study is that it proves that the ECG-derived VG is highly accurate in detecting chronic increase in RV pressure load, and as such can be used to distinguish between normal RV pressure load, mildly to moderately increased RV pressure load, and severely increased chronic RV pressure load. Furthermore, the ECG-derived VG proved to be of higher diagnostic accuracy for chronically increased RV pressure load than conventional ECG parameters. Available CMR data suggest that VG changes in PAH patients reflect changes in APD heterogeneity related to RV remodeling as a result of an increased RV pressure load.

Vectorcardiography vs. electrocardiography

The general approach towards ECG interpretation is one directed at individual leads overlying cardiac regions of interest, whereas each lead is derived from the same heart vector. Although a projection of the VG in a direction of interest is essentially a similar simplification of assessing a 3D process in time, this projection nevertheless holds all information derived from the two limb leads and six chest leads [9]. The vectorcardiogram takes into account that ECG leads have a different sensitivity (amongst others because of the variation in proximity to the heart) and does not suffer from the problem that onset QRS, end QRS, and end T instants may differ per lead [9]. The ECG-derived VG therefore renders robust results. Since calculation of the VG requires only straightforward integration over the QRST complex of the instantaneous heart vector (that can be synthesized from the ECG leads by a simple matrix multiplication) [18], this algorithm can easily be implemented in existing ECG analysis software, like we did in our LEADS program.

Despite the recognition of certain ECG characteristics in newborns and patients with an increased RV afterload, the diagnostic potential of conventional 12-lead ECG parameters for increased RV afterload has been reported as insufficient for clinical use or screening purposes [7, 25-27]. The results of our study support this view, yet underline the importance of using the full potential of an electrocardiogram. Contemporary software now renders (synthesized) vectorcardiogram-derived calculations with such ease that clinical application of this information is certainly feasible [17].

Rationale for using the VG

The VG is oriented towards the left and slightly antero-inferior in healthy human beings (Figure 2) within a smaller range than the mean QRS axis orientation in the frontal plane

[22]. The VG is the integrated ventricular APD heterogeneity, which is the 3D sum of the integrated ventricular depolarization and repolarization heterogeneities [10]. As such, the VG has a strong physiological link to the way in which the ventricular APD distribution is affected by chronic RV pressure load. Any intra-individual change in the VG magnitude and orientation signifies an alteration in APD heterogeneity in the ventricles, and hence a change in myocardial electrophysiological properties [10, 12]. Chou et al. evaluated the use of QRS loop area for diagnosis of RV hypertrophy [28]. As discussed by the authors, the QRS loop area is the sum of all depolarization vectors, allowing appreciation of the resultant spatial orientation and the ratio of leftward and rightward oriented forces, rendering evaluation of quantitative conventional ECG parameters of RV hypertrophy superfluous [28]. Cowdery et al. recognized the importance of the QRS loop area, and further improved diagnostic accuracy for RV hypertrophy by interpreting QRS amplitude in the transversal plane (60% sensitivity and 96% specificity) [29]. Kawaguchi et al. further concluded that repolarization characteristics should not be overlooked, since in their diagnostic model for RV hypertrophy combined T loop area and direction rendered the best result [30]. The high diagnostic accuracy for presence of chronic RV pressure load of the 3D VG (Figure 3), which is the sum of QRS and T integrals, is in accordance with these reports regarding changes in QRS complex and T wave morphology in patients with an increased RV pressure load [28-30].

There is a distinct evolution of ECG characteristics with developing PAH [13]. Changes in VG with increasing RV pressure load are best assessed in 3D, although single lead assessment is theoretically possible [11, 12]. Much like we observed in rats [13], a higher RV pressure load effectively cancels out the net LV contribution to the VG (Figure 1, lower panel) [13, 31, 32]. Obviously, this cancellation effect occurs because RV pressure load induced RV hypertrophy introduces APD heterogeneity substantially opposing the net LV APD heterogeneity. Thus, mild to moderate elevation of RV pressure load decreases VG magnitude, while VG orientation is largely maintained (Table 2, Figure 4). Further elevation of RV pressure load does not necessarily lead to a further decrease of VG magnitude, although it may drastically affect VG orientation (Figure 1, Figure 4, Table 2) [10]. A comparison with CMR studies in a subgroup of patients showed that RV pressure load induced changes in APD heterogeneity were related to changes in RV to LV mass ratio rather than to changes in RV to LV volume ratio. In steadily developing PAH, hypertrophy occurs already with mildly elevated pulmonary artery pressure, before dilatation of the RV is seen [13, 33]. This may explain the closer association of the VG projection on the X axis with RV hypertrophy rather than with RV dilatation.

Limitations

In the absence of available ECGs from the time before development of PAH we compared the ECGs of patients with a mildly to moderately elevated RV afterload as well as the ECGs of patients with a severely elevated RV afterload to the ECGs of healthy control subjects. Since we may assume that idiopathic PAH patients once had a normal RV afterload, comparison with ECGs from healthy individuals seems to be the most obvious alternative [34, 35]. This cross-sectional approach allows appreciation of the supposed evolution of changes in the VG in response to an increasing RV pressure load. The selection of patients with idiopathic PAH precludes application of our findings to patients with important lung disease or left-sided heart disease. However, since even a mildly to moderately elevated RV pressure load was associated with marked differences in the VG, the ECG seems a suitable screening tool for increased RV pressure load in selected groups of patients, such as relatives of patients with familial PAH, patients with HIV, systemic sclerosis, portal hypertension, or other diseases associated with development of PAH [7, 26]. Despite the obvious advantages of simply projecting the VG in the direction of interest (the X axis), a potential downside of this approach is the observed non-linear relation between PAH severity and the degree of chronic RV pressure load (Figure 4) which precludes classification of chronic RV pressure load beyond the categories of normal, mild to moderate, and severe RV pressure load. The size of our study group did not permit use of a learning set and test set. However, bootstrapping analysis confirmed the validity of the proposed predictive model of increased RV pressure load. The uneven sample sizes of mild to moderate PAH patients and severe PAH groups is suboptimal, yet a representative reflection of the high number of PAH patients with a mean PAP > 45mmHg at the time of diagnosis. The limited sample size of patients with mild to moderate PAH in our study may have affected the ability of the other ECG variables to discriminate between mild to moderate PAH and severe PAH.

Clinical implications

In patients with a genetic profile or disease known to predispose to PAH, serial ECG recording may prove a feasible concept for early detection of an increasing RV afterload. Apart from incorporation of calculations based on the VG into software for electrocardiographs, another way of indirectly assessing presence of chronic RV pressure load may be to calculate QRST areas in a lead with a lead vector that assumes about the direction of the X axis, such as lead I or V6. Whether such an individual lead-based VG approximation will prove to be of similar diagnostic accuracy deserves further study. Screening for PAH among patients at risk is still subject to debate, but is generally regarded as very costly due to the high rate of false

negative diagnoses with the available tools for non-invasive detection [36, 37]. The improved ECG detection of right ventricular pressure load using the VG may dramatically cut cost of screening. Whether sequential ECG recording allows for early distinction of 'responders' from 'non-responders' to PAH attenuating therapy by detection of VG changes, a distinction currently made by repetitive 6-minute walking tests, cardiac magnetic resonance imaging or right heart catheterization deserves further study [23, 38]. In patients without congenital or acquired left-sided heart disease and/or pulmonary disease the VG may prove to be an important tool for screening purposes and follow-up.

Conclusion

Chronically increased right ventricular pressure load induces changes in ventricular APD heterogeneity, which are reflected by distinct changes in the ventricular gradient. The ECG-derived ventricular gradient can be used with high accuracy for detection of chronically increased right ventricular pressure load, and is a potentially useful tool for follow-up in selected groups of patients. VG changes in PAH patients likely reflect changes in ventricular APD heterogeneity related to RV remodeling as a result of an increased RV pressure load.

References

1. Kosiborod M and Wackers FJ. Assessment of right ventricular morphology and function. Semin Respir Crit Care Med 2003;24:245-262.

2. Farb A, Burke AP and Virmani R. Anatomy and pathology of the right ventricle (including acquired tricuspid and pulmonic valve disease). Cardiol Clin 1992;10:1-21.

3. Chemla D, Castelain V, Herve P, Lecarpentier Y and Brimioulle S. Haemodynamic evaluation of pulmonary hypertension. Eur Respir J 2002;20:1314-1331.

4. Harrigan RA and Jones K. ABC of clinical electrocardiography. Conditions affecting the right side of the heart. BMJ 2002;324:1201-1204.

5. Sukhija R, Aronow WS, Ahn C and Kakar P. Electrocardiographic abnormalities in patients with right ventricular dilation due to acute pulmonary embolism. Cardiology 2006;105:57-60.

6. Punukollu G, Gowda RM, Vasavada BC and Khan IA. Role of electrocardiography in identifying right ventricular dysfunction in acute pulmonary embolism. Am J Cardiol 2005;96:450-452.

7. McGoon M, Gutterman D, Steen V, Barst R, McCrory DC, Fortin TA and Loyd JE. Screening, early detection, and diagnosis of pulmonary arterial hypertension: ACCP evidence-based clinical practice guidelines. Chest 2004;126:14S-34S.

8. Barst RJ, McGoon M, Torbicki A, Sitbon O, Krowka MJ, Olschewski H and Gaine S. Diagnosis and differential assessment of pulmonary arterial hypertension. J Am Coll Cardiol 2004;43:40S-47S.

9. MacFarlane PW, Edenbrandt L and Pahlm O. 12 Lead Vectorcardiography. Oxford: Butterworth-Heinemann, 1995.

10. Draisma HH, Schalij MJ, van der Wall EE and Swenne CA. Elucidation of the spatial ventricular gradient and its link with dispersion of repolarization. Heart Rhythm 2006;3:1092-1099.

11. Hurst JW. Thoughts about the ventricular gradient and its current clinical use (Part I of II). Clin Cardiol 2005;28:175-180.

12. Hurst JW. Thoughts about the ventricular gradient and its current clinical use (part II of II). Clin Cardiol 2005;28:219-224.

13. Henkens IR, Mouchaers K, Vliegen HW, van der Laarse WJ, Swenne CA, Maan AC, Draisma HH, Schalij I, van der Wall EE, Schalij MJ and Vonk Noordegraaf A. Early changes in rat hearts with developing pulmonary arterial hypertension can be detected with 3-dimensional electrocardiography. Am J Physiol Heart Circ Physiol 2007;

14. Kim NH. Diagnosis and evaluation of the patient with pulmonary hypertension. Cardiol Clin 2004;22:367-3vi.

15. Mirvis DM and Goldberger AL. Electrocardiography. In: Braunwald's Heart Disease, edited by Zipes DP, Libby P, Bonow RO and Braunwald E. Saunders, 2004, p. 120-125.

16. Galie N, Torbicki A, Barst R, Dartevelle P, Haworth S, Higenbottam T, Olschewski H, Peacock A, Pietra G, Rubin LJ, Simonneau G, Priori SG, Garcia MA, Blanc JJ, Budaj A, Cowie M, Dean V, Deckers J, Burgos EF, Lekakis J, Lindahl B, Mazzotta G, McGregor K, Morais J, Oto A, Smiseth OA, Barbera JA, Gibbs S, Hoeper M, Humbert M, Naeije R and Pepke-Zaba J. Guidelines on diagnosis and treatment of pulmonary arterial hypertension. The Task Force on Diagnosis and Treatment of Pulmonary Arterial Hypertension of the European Society of Cardiology. Eur Heart J 2004;25:2243-2278.

17. Draisma HH, Swenne CA and Van de Vooren H. LEADS: an interactive research oriented ECG/VCG. Computers in Cardiology 2005;32:515-518.

18. Edenbrandt L and Pahlm O. Vectorcardiogram synthesized from a 12-lead ECG: superiority of the inverse Dower matrix. J Electrocardiol 1988;21:361-367.

19. Burger HC. A theoretical elucidation of the notion ventricular gradient. Am Heart J 1957;53:240-246.

20. Kossmann CE, Brody DA, Burch GE, Hecht HE, Johnston FD, Kay C, Lepeschkin E, Pipberger HV, Baule G, Berson AS, Briller SA, Geselowitz DB, Horan LG and Schmitt OH. Report of committee on electrocardiography, American Heart Association. Recommendations for standardization of leads and of specifications for instruments in electrocardiography and vectorcardiography. Circulation 1967;35:583-602.

21. Blackburn H. Electrocardiographic classification for population comparisons. The Minnesota code. J Electrocardiol 1969;2:5-9.

22. Yano K and Pipberger HV. Spatial magnitude, orientation, and velocity of the normal and abnormal QRS complex. Circulation 1964;29:107-117.

23. van Wolferen SA, Marcus JT, Boonstra A, Marques KM, Bronzwaer JG, Spreeuwenberg MD, Postmus PE and Vonk Noordegraaf A. Prognostic value of right ventricular mass, volume, and function in idiopathic pulmonary arterial hypertension. Eur Heart J 2007;28:1250-1257.

24. Hanley JA and McNeil BJ. A method of comparing the areas under receiver operating characteristic curves derived from the same cases. Radiology 1983;148:839-843.

25. Rich S, Dantzker DR, Ayres SM, Bergofsky EH, Brundage BH, Detre KM, Fishman AP, Goldring RM, Groves BM and Koerner SK. Primary pulmonary hypertension. A national prospective study. Ann Intern Med 1987;107:216-223.

26. Ahearn GS, Tapson VF, Rebeiz A and Greenfield JC, Jr. Electrocardiography to define clinical status in primary pulmonary hypertension and pulmonary arterial hypertension secondary to collagen vascular disease. Chest 2002;122:524-527.

27. Penaloza D and Arias-Stella J. The heart and pulmonary circulation at high altitudes: healthy highlanders and chronic mountain sickness. Circulation 2007;115:1132-1146.

28. Chou TC, Masangkay MP, Young R, Conway GF and Helm RA. Simple quantitative vectorcardiographic criteria for the diagnosis of right ventricular hypertrophy. Circulation 1973;48:1262-1267.

29. Cowdery CD, Wagner GS, Starr JW, Rogers G and Greenfield JC, Jr. New vectorcardiographic criteria for diagnosing right ventricular hypertrophy in mitral stenosis: comparison with electrocardiographic criteria. Circulation 1980;62:1026-1032.

30. Kawaguchi Y. Studies on deflection area vectors of QRS and T and ventricular gradient in right ventricular hypertrophy. Jpn Circ J 1985;49:395-405.

31. Abildskov JA, Burgess MJ, Millar K, Wyatt R and Baule G. The primary T wave a new electrocardiographic waveform. Am Heart J 1971;81:242-249.

32. Burgess MJ, Millar K and Abildskov JA. Cancellation of electrocardiographic effects during ventricular recovery. J Electrocardiol 1969;2:101-107.

33. Vonk Noordegraaf A, Marcus JT, Holverda S, Roseboom B and Postmus PE. Early changes of cardiac structure and function in COPD patients with mild hypoxemia. Chest 2005;127:1898-1903.

34. Rubin LJ. Pathology and pathophysiology of primary pulmonary hypertension. Am J Cardiol 1995;75:51A-54A.

35. Perros F, Dorfmuller P and Humbert M. Current insights on the pathogenesis of pulmonary arterial hypertension. Semin Respir Crit Care Med 2005;26:355-364.

36. Mukerjee D, St GD, Knight C, Davar J, Wells AU, Du Bois RM, Black CM and Coghlan JG. Echocardiography and pulmonary function as screening tests for pulmonary arterial hypertension in systemic sclerosis. Rheumatology (Oxford) 2004;43:461-466.

37. Williams MH, Handler CE, Akram R, Smith CJ, Das C, Smee J, Nair D, Denton CP, Black CM and Coghlan JG. Role of N-terminal brain natriuretic peptide (N-TproBNP) in scleroderma-associated pulmonary arterial hypertension. Eur Heart J 2006;27:1485-1494.

38. Kawut SM and Palevsky HI. Surrogate end points for pulmonary arterial hypertension. Am Heart J 2004;148:559-565.